**Geomechanics and Engineering**, *Vol. 14, No. 4 (2018) 315-324*
DOI: https://doi.org/10.12989/gae.2018.14.4.315


# A multivariate adaptive regression splines model for estimation of maximum wall deflections induced by braced excavation

Yuzhou Xiang[1], Anthony Teck Chee Goh[2], Wengang Zhang[*1,3] and Runhong Zhang[4]

[1]*School of Civil Engineering, Chongqing University, Chongqing 400045, China*
[2]*School of Civil and Environmental Engineering, Nanyang Technological University, 639798, Singapore*
[3]*Key Laboratory of New Technology for Construction of Cities in Mountain Area, Chongqing University, China*
[4]*School of Civil and Environmental Engineering, Nanyang Technological University, 639798, Singapore*

*(Received August 17, 2018, Revised July 11, 2017, Accepted August 8, 2017)*

**Abstract.** With rapid economic growth, numerous deep excavation projects for high-rise buildings and subway transportation networks have been constructed in the past two decades. Deep excavations particularly in thick deposits of soft clay may cause excessive ground movements and thus result in potential damage to adjacent buildings and supporting utilities. Extensive plane strain finite element analyses considering small strain effect have been carried out to examine the wall deflections for excavations in soft clay deposits supported by diaphragm walls and bracings. The excavation geometrical parameters, soil strength and stiffness properties, soil unit weight, the strut stiffness and wall stiffness were varied to study the wall deflection behaviour. Based on these results, a multivariate adaptive regression splines model was developed for estimating the maximum wall deflection. Parametric analyses were also performed to investigate the influence of the various design variables on wall deflections.

**Keywords:** wall deflection; braced excavation; multivariate adaptive regression splines; case histories; parametric analysis; finite element analysis

## 1. Introduction

Wall deflection and ground settlement generally occur as a result of cut-and-cover excavation to construct underground structures such as basement car parks and subway stations. Excessive ground settlement can frequently result in damage the adjacent buildings in urban areas. The magnitude of the wall deflection and ground settlement associated with deep excavations is generally dependent on the excavation geometry, the type of support system, the properties of the in situ soils, and the excavation procedure. For excavations in ground that comprises of thick soft clays overlying stiff clay, braced walls are usually used to minimize ground movements. It is common to extend the wall toe sufficiently into the stiff clay layer to prevent basal heave failure and also to reduce the movement of the wall toe. To ensure the serviceability limit state is not exceeded, a common design criterion is to limit the maximum wall deflection to a fraction of the excavation depth $H_e$, generally in the range of 0.05% to more than 2% of the excavation depth $H_e$ (Yoo and Kim 1999, Long 2001, Moormann 2004). Unnecessarily severe restrictions will lead to uneconomic wall designs. Therefore, reliable estimates of wall deflections under working conditions are essential.

The finite element (or finite difference) method, the analytical method, and the empirical/semi-empirical method are three common approaches for estimating wall deflections induced by excavation. The finite element method is widely employed to model complex soil-structure interaction problems and the associated sequential excavations. For excavations in soft clays, the commonly used Mohr-Coulomb (MC) constitutive relationship may not always properly model the clay stress-strain behaviour, when the soil small strain effect is neglected. The importance of modelling the soil small strain behaviour for many geotechnical problems has been highlighted by Burland (1989) and Jardine *et al.* (1986). The influence of the soil small strain effect on excavation problems (Benz 2007, Osman and Bolton 2006, Kung *et al.* 2009, Hsieh *et al.* 2016), have demonstrated improvements in the predictions of wall deflection and ground movement.

Empirical and semi-empirical methods involve interpolating from a published empirical database or from data obtained from finite element analyses. Several empirical and semi-empirical methods are available for estimating the excavation-induced maximum wall deflection (Mana and Clough 1981, Wong and Broms 1989, Clough and O'Rourke 1990, Hashash and Whittle 1996, Addenbrooke *et al.* 2000, Ukritchon *et al.* 2003, Son and Cording 2005, Kung *et al.* 2007a, Wang *et al.* 2010, Koutsoftas 2012, Hsieh *et al.* 2012, Whittle *et al.* 2014, Zhang *et al.* 2015, Hsieh and Ou 2016, Hsiung *et al.* 2016, Zhang and Goh 2016, Goh *et al.* 2017). However, many of these methods that have been proposed for estimating wall movements assume that the wall is "floating" in the soft clay, without restraint at the wall toe. This paper focuses on

∗Corresponding author, Professor
E-mail: cheungwg@126.com

**Copyright © 2018 Techno-Press, Ltd.**

ISSN: 2005-307X (Print), 2092-6219 (Online)

the specific situation of the braced wall penetrating into the stiff stratum, since as mentioned previously it is common to extend the wall length sufficiently into the stiff clay layer to prevent basal heave failure and to reduce the movement of the wall toe.

In this paper, parametric studies were carried out using the plane strain finite element (FE) software Plaxis (Brinkgreve *et al.* 2006) in which the soft clay stress-strain behaviour was modelled using the hardening small strain (HSS) constitutive relationship that considers the small strain effect in consideration that the braced excavations are generally conservatively designed, which indicates that actually at low strain levels most soils exhibit a higher stiffness than at engineering strain levels. Analyses were carried out to evaluate the behaviour of excavations with braced walls in soft clays. Based on the numerical modelling results, this paper describes the use of a multivariate adaptive regression splines (MARS) model for relating the maximum wall deflection to various design parameters such as the excavation geometry, soil strength and stiffness properties, soil unit weight, the strut stiffness and wall stiffness.

## 2. MARS methodology

Friedman (1991) introduced MARS as a statistical method for fitting the relationship between a set of input variables and dependent variables. It is a nonlinear and nonparametric regression method based on a divide and conquer strategy in which the training data sets are partitioned into separate piecewise linear segments (splines) of differing gradients (slope). No specific assumption about the underlying functional relationship between the input variables and the output is required. The end points of the segments are called knots. A knot marks the end of one region of data and the beginning of another. The resulting piecewise curves (known as basis functions), give greater flexibility to the model, allowing for bends, thresholds, and other departures from linear functions.

MARS generates basis functions by searching in a stepwise manner. An adaptive regression algorithm is used for selecting the knot locations. MARS models are constructed in a two-phase procedure. The forward phase adds functions and finds potential knots to improve the performance, resulting in an overfit model. The backward phase involves pruning the least effective terms. An open source code on MARS from Jekabsons (2010) is used in carrying out the analyses presented in this paper.

Let $y$ be the target output and $\boldsymbol{X} = (X_1, \ldots, X_P)$ be a matrix of $P$ input variables. Then it is assumed that the data are generated from an unknown "true" model. In case of a continuous response this would be

$$y = f(X_1, \ldots, X_P)+e= f(\boldsymbol{X})+e \tag{1}$$

in which $e$ is the distribution of the error. MARS approximates the function $f$ by applying basis functions (BFs). BFs are splines (smooth polynomials), including piecewise linear and piecewise cubic functions. For simplicity, only the piecewise linear function is expressed. Piecewise linear functions are of the form max(0,$x-t$) with a knot occurring at value $t$. The equation max(.) means that only the positive part of (.) is used otherwise it is given a zero value. Formally,

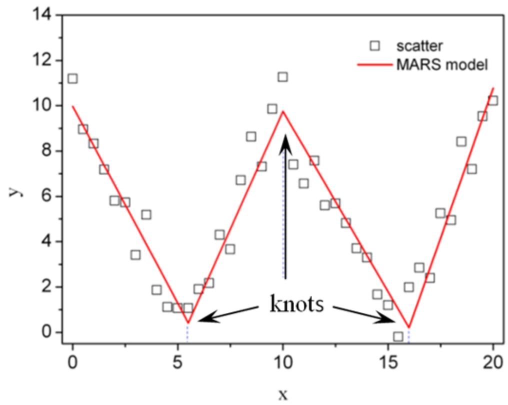


Fig. 1 Knots and linear splines for a simple MARS example

$$\max(0, x-t) = \begin{cases} x-t, if\ x \geq t \\ 0, otherwise \end{cases} \tag{2}$$

The MARS model $f(X)$ is constructed as a linear combination of BFs and their interactions, and is expressed as

$$f(X) = \beta_0 + \sum_{m=1}^{M} \beta_m \lambda_m(X) \tag{3}$$

where each $\lambda m(x)$ is a basis function. It can be a spline function, or the product of two or more spline functions already contained in the model (higher orders can be used when the data warrants it; for simplicity, at most second-order is assumed in this paper). The coefficients $\beta$ are constants, estimated using the least-squares method.

Fig. 1 shows a simple example of how MARS would use piecewise linear spline functions to attempt to fit data. The MARS mathematical equation is expressed as

$$y = -44.08 + 4.24 \times BF1 - 3.67 \times BF2 + 6.31 \times BF3 - 2.50 \times BF4 \tag{4}$$

where $BF1$=max(0, 16–$x$), BF2=max(0, $x$–10), BF3=max(0, $x$–5.5) and BF4=max(0, 5.5–$x$). The knots are located at $x$ = 5.5, 10 and 16. They delimit four intervals where different linear relationships are identified. It is obvious that the MARS approach is good at analyzing problems in which there is significant scatter in both the explanatory independent variables and the target responses.

The MARS modelling is a data-driven process. To fit the model in Eq. (3), first a forward selection procedure is performed on the training data. A model is constructed with only the intercept, $\beta_0$, and the basis pair that produces the largest decrease in the training error is added. Considering a current model with $M$ basis functions, the next pair is added to the model in the form

$$\hat{\beta}_{M+1} \lambda_m(X) \max(0, X_j - t) + \hat{\beta}_{M+2} \lambda_m(X) \max(0, t - X_j) \tag{5}$$

with each $\beta$ being estimated by the method of least squares. As a basis function is added to the model space, interactions between BFs that are already in the model are also considered. BFs are added until the model reaches some maximum specified number of terms leading to a purposely overfit model.

To reduce the number of terms, a backward deletion sequence follows. The aim of the backward deletion procedure is to find a close to optimal model by removing extraneous variables. The backward pass prunes the model by removing the BFs with the lowest contribution to the model until it finds the best sub-model. Thus, the BFs maintained in the final optimal model are selected from the set of all candidate BFs, used in the forward selection step. Model subsets are compared using the less computationally expensive method of Generalized Cross-Validation (GCV). The GCV equation is a goodness of fit test that penalizes large numbers of BFs and serves to reduce the chance of overfitting. For the training data with $N$ observations, GCV for a model is calculated as follows (Hastie *et al.* 2009)

$$GCV = \frac{\frac{1}{N}\sum_{i=1}^{N}[y_i - f(x_i)]^2}{[1-\frac{M+d\times(M-1)/2}{N}]^2} \tag{6}$$

in which $M$ is the number of BFs, $d$ is the penalizing parameter, $N$ is the number of observations, and $f(x_i)$ denotes the predicted values of the MARS model. The numerator is the mean squared error of the evaluated model in the training data, penalized by the denominator. The denominator accounts for the increasing variance in the case of increasing model complexity. Note that $(M-1)/2$ is the number of hinge function knots. The GCV penalizes not only the number of the model's basis functions but also the number of knots. A default value of 3 is assigned to penalizing parameter $d$ (Friedman 1991). At each deletion step a basis function is removed to minimize Eq. (3), until an adequately fitted model is found. MARS is an adaptive procedure because the selection of BFs and the variable knot locations are data-based and specific to the problem at hand.

After the optimal MARS model is determined, by grouping together all the BFs that involve one variable and another grouping of BFs that involve pair-wise interactions (and even higher level interactions when applicable), the procedure known as analysis of variance (ANOVA) decomposition (Friedman 1991) can be used to assess the contributions from the input variables and the BFs through comparing (testing) variables for statistical significance. Previous applications of MARS algorithm in civil engineering can be found in Attoh-Okine *et al.* (2009), Zarnani *et al.* (2011), Samui and Karup (2011), Lashkari (2012), Zhang and Goh (2013), Adoko *et al.* (2013), Goh and Zhang (2014), Khoshnevisan *et al.* (2015). Zhang *et al.* (2015), Goh *et al.* (2016), Zhang *et al.* (2017).

## 3. Soil model

The hardening-soil (HS) model (Brinkgreve and Vermeer 1997, Schanz *et al.* 1999) is an advanced constitutive model for simulating the behaviour of soils. The model involves frictional hardening characteristics to model plastic shear strain in deviatoric loading, and cap hardening to model plastic volumetric strain in primary compression. Failure is defined by the Mohr-Coulomb failure criterion. The main input parameters are $E_{50}^{ref}$, a reference secant modulus corresponding to the reference confining pressure $p^{ref}$, a power $m$ for stress-dependent stiffness formulation, effective friction angle cohesion $c$, failure ratio $R_f$, $E_{ur}^{ref}$ the reference stiffness modulus for unloading and reloading corresponding to $p^{ref}$, and $\upsilon_{ur}$ the unloading and reloading Poisson's ratio. This model has been used for analyses of deep excavations by a number of researchers including Finno and Calvello (2005) and Bryson and Zapata-Medina (2005).

The main parameters of the HSS model include $G_0^{ref}$, $\phi$, and $E_{50}^{ref}$. $G_0^{ref}$ is a reference initial shear stiffness corresponding to the reference pressure $p^{ref}$ and shear strain $\gamma_{0.7}$ at which the secant shear modulus is reduced to 70% of $G_0$. Following the approach recommended by Brinkgreve *et al.* (2006), $G_0^{ref}$ was obtained by first determining the $E_0/E_{ur}$ ratio based on the chart by Alpan (1970) and assuming $E_{ur} = 3E_{50}$, where $E_0$ is the small strain Young's modulus, and subsequently using the expression $G_0^{ref} = E_0^{ref}/(2(1+\upsilon_{ur}))$ with $\upsilon_{ur}$ assumed as a constant. Since the chart for estimating the parameter $\gamma_{0.7}$ based on Vucetic and Dobry (1991) and reported in Brinkgreve *et al.* (2006) shows that $\gamma_{0.7}$ only varies within a narrow range between $1\times10^{-4}$ and $4\times10^{-4}$, in this paper $\gamma_{0.7}=2\times10^{-4}$ was assumed. The $G_0$ is defined as

$$G_0 = G_0^{ref}\left(\frac{c'cos\phi - \sigma_3' sin\phi}{c'cos\phi + p^{ref} sin\phi}\right)^m \tag{7}$$

where $\sigma'_3$ is the effective confining stress (assuming compressive stress is negative). The effective friction angle $\phi$ is computed using the correlation proposed by Wroth and Houlsby (1985)

$$\frac{c_u}{\sigma_v'} = 0.5743\frac{3sin\phi}{3-sin\phi} \tag{8}$$

in which $c_u$ is the undrained shear strength and $\sigma'_v$ is the vertical effective stress. When the ground water table is at the ground surface and assuming $m$=1, $c_u/\sigma'_v = \alpha$, soil stiffness ratio $E_{50}/c_u = \beta$ and $\sigma_3' = K_0\sigma_1'$ in the HSS model, $E_{50}^{ref}$ can be expressed as

$$E_{50}^{ref} = \frac{E_{50}}{(\frac{\sigma_3'}{p^{ref}})^m} = \frac{\alpha c_u}{(\frac{K_0\times c_u}{\beta\times p^{ref}})^m} = \frac{\alpha\beta p^{ref}}{K_0} \tag{9}$$

The HSS model accounts for the increased stiffness of soils at small strains. At low strain levels most soils exhibit a higher stiffness than at engineering strain levels, and this stiffness varies non-linearly with strain. In the TNEC case history back analysis, Kung *et al.* (2009) used a small-strain constitutive model as well as a Modified Cam Clay (MCC) model for soft/medium clay. Their results indicated that the small-strain model was able to predict the wall lateral deflection and ground surface settlement fairly well, but that the MCC model could not predict accurately the surface settlement. Other publications in which small strain has been used to model excavation in soft/medium clay include Hashash and Whittle (1996), Borja *et al.* (1997), Rampello *et al.* (1997), Jen (1998), Kung (2003), Finno and Tu (2006), Kung *et al.* (2007b), Lam (2010), Clayton (2011), and Lashkari and Mahboubi (2015).

The Plaxis default values are used to define the power for stress-level dependency of the stiffness $m$, the coefficient of earth pressure at-rest $K_0^{nc}$, the Poisson's ratio $\upsilon_{ur}$ and $E_{ur}$ with $m$=1, $K_0^{nc}$=1–sin$\phi$, $\upsilon_{ur}$=0.2 and $E_{ur}$=3$E_{50}$.

## 4. Finite element analyses and parametric studies

Parametric studies have been carried out using the HSS model for the soft clay with emphasis on the maximum wall deflection predictions. Fig. 2 shows schematically the cross section of the excavation system, with a slightly simplified soil profile comprising of a thick normally consolidated soft clay layer overlying a stiff clay layer, typical of soil conditions in many coastal areas. The Mohr-Coulomb constitutive relationship was used to model the stiff clay ($\gamma$=20 kN/m$^3$, $c_u$=500 kPa, $E_u$=250 MPa) underlying the soft clay deposit. The soft clay thickness is denoted as $T$ and $H_e$ is the final excavation depth in Fig. 2. The penetration depth of the wall into the stiff layer was varied between 3 and 5 m. Results indicated minimal differences in the wall deflections for these penetration depths.

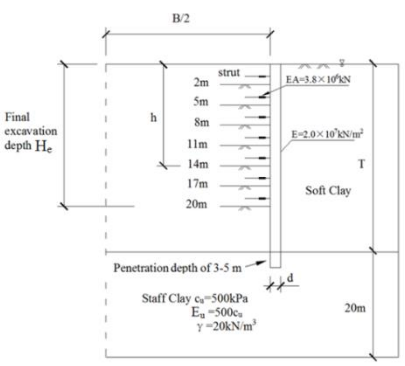


Fig. 2 Cross-sectional soil and wall profile

Table 1 Range of parameters

| Parameter | Range |
|---|---|
| Relative soil shear strength ratio $c_u/\ \ '_v$ | 0.21, 0.25, 0.29, 0.34 |
| Relative soil stiffness ratio $E_{50}/c_u$ | 100, 200, 300 |
| Soil unit weight (kN/m$^3$) | 15, 17, 19 |
| Soft clay thickness $T$ (m) | 25, 30, 35 |
| Excavation width $B$ (m) | 20,30, 40, 50, 60 |
| Excavation depth $H_e$ (m) | 11, 14, 17, 20 |
| Wall stiffness $EI$ (× 10$^6$kN·m$^2$/m) | 0.36, 1.21, 2.88, 5.63 |

Table 2 $\phi$ and K0values for soft clay in HSS model

| $c_u/\sigma'_v$ | 0.21 | 0.25 | 0.29 | 0.34 |
|---|---|---|---|---|
| $\phi$(°) | 19 | 22.3 | 25.6 | 29.6 |
| $K_0$ | 0.674 | 0.621 | 0.568 | 0.506 |

Table 3 E50$^{ref}$ values for soft clay in HSS model

| $c_u/\sigma'_v$ | $E_{50}^{ref}$ (kPa) | | | |
|---|---|---|---|---|
| | $E_{50}/c_u = 100$ | $E_{50}/c_u = 200$ | $E_{50}/c_u = 300$ | $E_{50}/c_u = 400$ |
| 0.21 | 3114 | 6228 | 9342 | 12456 |
| 0.25 | 4031 | 8062 | 12093 | 16124 |

Table 3 Continued

| $c_u/\sigma'_v$ | $E_{50}^{ref}$ (kPa) | | | |
|---|---|---|---|---|
| | $E_{50}/c_u = 100$ | $E_{50}/c_u = 200$ | $E_{50}/c_u = 300$ | $E_{50}/c_u = 400$ |
| 0.29 | 5105 | 10210 | 15315 | 20420 |
| 0.34 | 6721 | 13442 | 20163 | 26884 |

The analyses considered a plane strain excavation supported by a retaining wall system. Considering symmetry, only half the cross-section was considered. The soil was modelled by 15-noded triangular elements. The structural elements were assumed to be linear elastic with the wall represented by 5-noded beam elements and 3-noded bar elements were used for the 7 levels of struts located at depths of 1 m, 4 m, 7 m, 10 m, 13 m, 16 m and 19 m below the original ground surface. The nodes along the side boundaries of the mesh were constrained from displacing horizontally while the nodes along the bottom boundary were constrained from moving horizontally and vertically. The right vertical boundary extends far from the excavation to minimize the effects of the boundary restraints. The ranges of properties varied are shown in Table 1. The various $\phi$, $K_0$, and $E_{50}^{ref}$ values derived from empirical equations in section 2 are listed in Tables 2 and 3, respectively.

The influence of the wall stiffness was studied by varying the wall thickness $d$ while keeping the Young's modulus of the wall constant ($E$ = 2.0×10$^7$ kN/m$^2$). The corresponding natural logarithm of the system stiffness ln$(EI/\gamma_w h_{avg}^4)$(denoted as ln($S$) in the following sections for brevity) for the wall thickness of 0.6, 0.9, 1.2 and 1.5 m with average vertical strut spacing $h_{avg}$=3 m are 6.097, 7.313, 8.176, and 8.846, respectively.

The strut stiffness per meter $(EA)_{strut}$ is assumed as a constant at 1.0×10$^6$kN/m since the influence of $(EA)_{strut}$ on wall deflection is not very significant when the strut is stiff (Poh and Wong 1997). However, taking into account the excavation width, the strut stiffness parameter $k_{strut}$ is introduced as

$$k_{strut} = \frac{(EA)_{strut}}{ls} = \frac{(EA)_{strut}}{(B/2)s} = \frac{2(EA)_{strut}}{Bs} \tag{10}$$

where $k_{strut}$=stiffness of strut; $(EA)_{strut}$ is the strut stiffness per meter, $l$=half-length of each strut; and $s$=horizontal spacing of each strut. For $l$=10 m (i.e., if the excavation is symmetrical with width $B$=20 m)

The construction sequence comprised the following steps:

(1) the wall is installed ("wished into place") without any disturbance in the surrounding soil;

(2) the soil is excavated uniformly 1 m below each strut level prior to adding the strut support with struts at 3 m vertical spacing until the final depth $H_e$ is reached. The soil is assumed to be subjected to undrained shearing (undrained analysis method A in Plaxis) during excavation. Analyses were performed assuming the groundwater table to be at the original ground surface.

Fig. 3 presents the wall deflections corresponding to different excavation stages ($h$ denotes the depth of

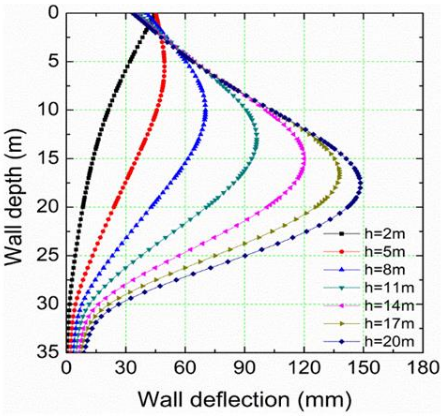


Fig. 3 Wall deflection profile for different excavation stage

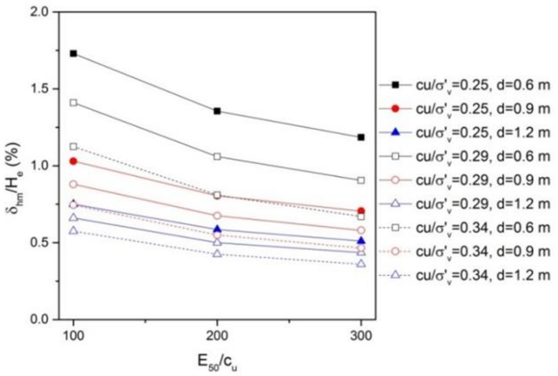


Fig. 4 Effect of soil stiffness on normalized wall deflection for $H_e$=20 m, $\gamma$=17 kN/m$^3$, $B$=30 m and $T$=30 m)

excavation) for the case of $k_{strut}$=31667 kN/m$^2$, $H_e$=20 m, $c_u/\sigma'_v$=0.29, $E_{50}/c_u$=200, $\gamma$=17 kN/m$^3$, ln($S$) =7.313 and $T$=30 m with a penetration depth of 5 m. The cantilever wall deflection profile (h=2 m) can be observed at first excavation stage (prior to installation of the top level strut). The diaphragm wall then displays deep inward movements at subsequent stages. The maximum wall deflection $\delta_{hm}$ increases as excavation proceeds.

The influence of the soil stiffness ratio $E_{50}/c_u$ and system stiffness ln($S$) (denoted by wall thickness) is shown in Fig. 4 for cases with $\gamma$=17 kN/m$^3$, $k_{strut}$=42222 kN/m$^2$, and $T$=30 mfor $c_u/\sigma'_v$=0.25, 0.29, and 0.34, respectively. It is obvious that the normalized wall deflection decreases with the increase of the relative soil stiffness ratio $E_{50}/c_u$. In addition, the influence of $E_{50}/c_u$ is more significant for lower wall thickness $d$. For the same system stiffness (same $d$), the normalized wall deflection decreases with the increase of relative soil shear strength ratio $c_u/\sigma'_v$.

The influence of strut stiffness $k_{strut}$ for the cases with $H_e$=20 m, $c_u/\sigma'_v$=0.34, $d$ =0.9 m is presented in Fig. 5 for $E_{50}/c_u$ =100, 200 and 300, respectively. The results show the normalized maximum wall deflection decreases with the increase of the strut stiffness. It is also obvious that the normalized wall deflection increases with the increase of the soft clay thickness $T$. In addition, the influence of soil the influence of strut stiffness $k_{strut}$ for the cases with $H_e$=20 m, $c_u/\sigma'_v$=0.34, $d$ =0.9 m is presented in Fig. 5 for

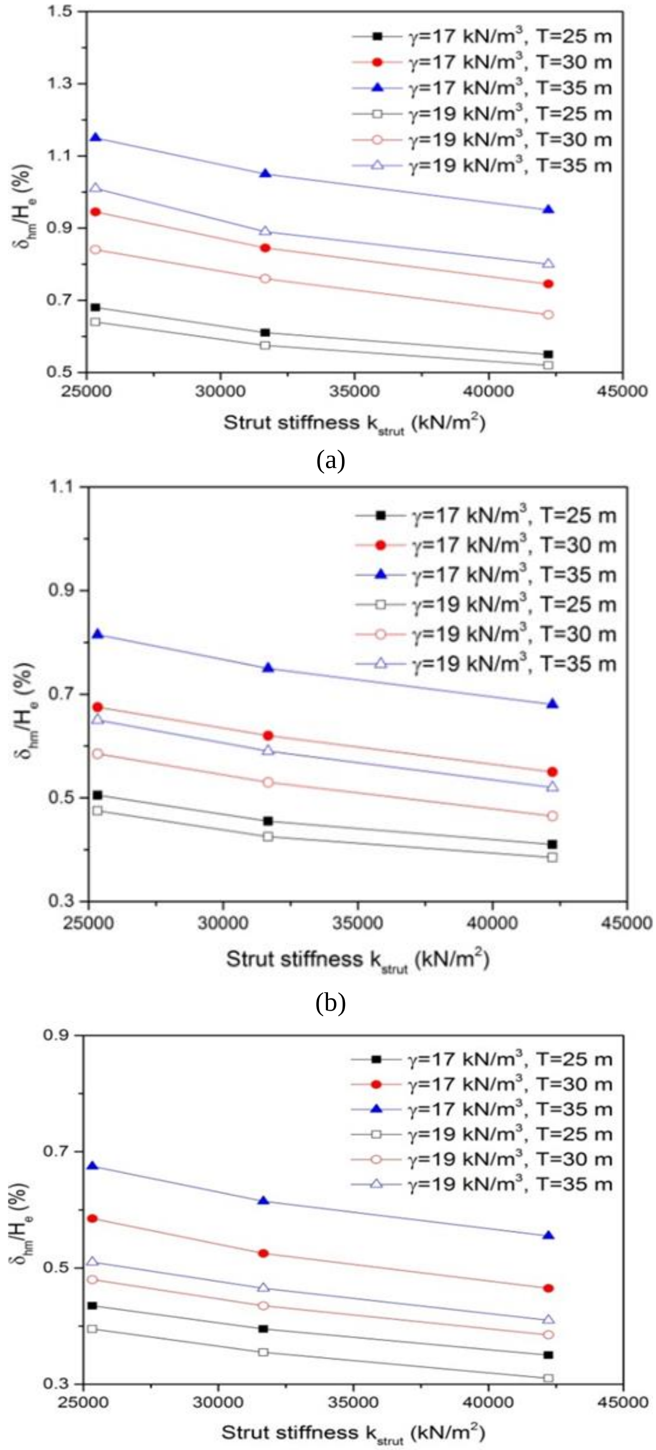


(a)

(b)

(c)

Fig. 5 Effect of strut stiffness $k_{strut}$ on normalized wall deflection for (a) $E_{50}/c_u$=100, (b) $E_{50}/c_u$=200, and (c) $E_{50}/c_u$=300 ($c_u/\sigma'_v$= 0.34, $d$=0.9 m, and $H_e$=20 m)

$E_{50}/c_u$ =100, 200 and 300, respectively. The results show the normalized maximum wall deflection decreases with the increase of the strut stiffness. It is also obvious that the normalized wall deflection increases with the increase of the soft clay thickness $T$. In addition, the influence of soil unit weight $\gamma$ is more significant for larger soft clay thickness $T$.

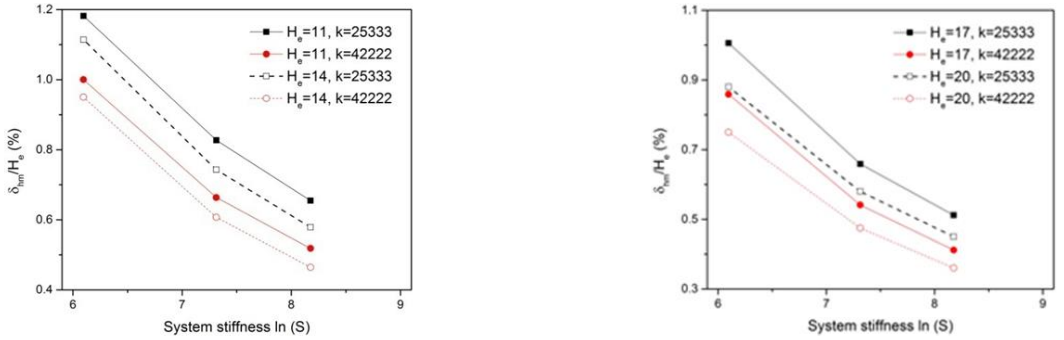


(a) T=25 m

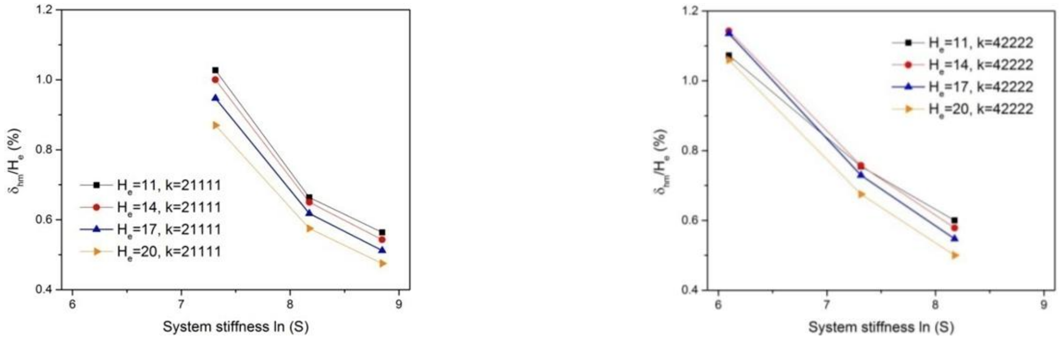


(b) T=30 m

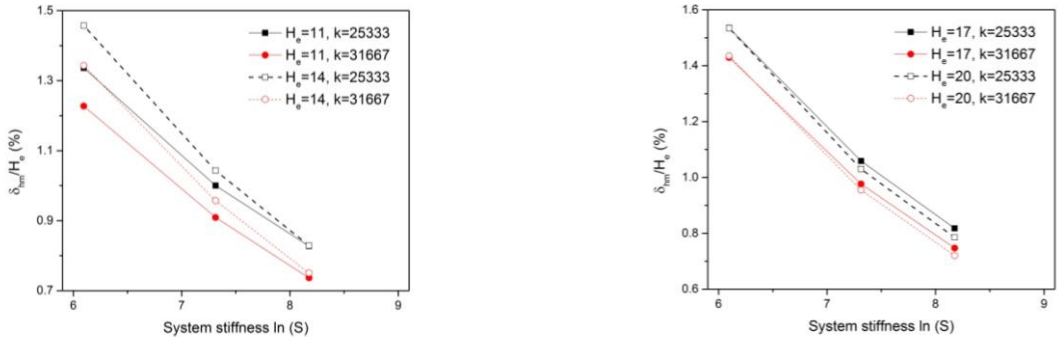


(c) T=35 m

Fig. 6 Effect of excavation depth He on normalized wall deflection for (a) T=25 m, (b) T=30 m and (c) T=35 m ($c_u/\sigma'_v$=0.29, E50/cu = 200, and $\gamma$= 17 kN/m$^3$)

The influences of both the wall stiffness and the strut stiffness for the cases with $\gamma$=17 kN/m$^3$, $E_{50}/c_u$=200, $c_u/\sigma'_v$=0.29 is presented in Fig. 6(a)-6(c) for $T$ =25 m, 30 m and 35 m, respectively. Fig. 6(a) shows the normalized wall deflection $\delta_{hm}/H_e$ for $k_{strut}$=25333 and 42222 (strut moderately stiff and very stiff). It is obvious from Fig. 6(a) that $\delta_{hm}/H_e$ decreases with the increase of the system stiffness ln($S$) and the strut stiffness $k_{strut}$. Fig. 6(b) shows the normalized wall deflection $\delta_{hm}/H_e$ for $k_{strut}$=21111 and 42222 (strut less stiff and very stiff). It is obvious from Fig. 6(b) for less stiff strut, to keep the $\delta_{hm}/H_e$ within a reasonable limit, the system stiffness ln(S) must increase accordingly. In addition, it can be observed that for very stiff strut, the influence of excavation depth $H_e$ on $\delta_{hm}/H_e$ is less significant while the influence of system stiffness is still considerable. Fig. 6(c) shows the normalized wall deflection $\delta_{hm}/H_e$ for v= 25333 and 31667 (strut moderately stiff and stiff) with a great thickness of soft soil. It is obvious from Fig. 6(c) that the influence of excavation depth $H_e$ on $\delta_{hm}/H_e$ is becoming less significant as the system stiffness increases for $H_e$=11 and 14 m. The difference of $\delta_{hm}/H_e$ is marginal even when the system stiffness ln(S) is at a small value of 6.097.

Based on Figs. 4-6, it is obvious that $\delta_{hm}/H_e$ is significantly influenced by excavation geometries $T$, $B$ and $H_e$, soil parameters $c_u/\sigma'_v$, $E_{50}/c_u$ and $\gamma$, strut and wall stiffness $k_{strut}$ and ln(S). Thus, estimation of $\delta_{hm}/H_e$ is a multivariate geotechnical problem.

## 5. The developed MARS model

A total of 1120 hypothetical cases were analyzed (Xuan 2009). Based on the results, a MARS model has been developed for estimating the normalized maximum wall deflection $\delta_{hm}/H_e$ (%) as a function of six input parameters: $\gamma$, $k_{strut}$, $c_u/\sigma'_v$, $E_{50}/c_u$, system stiffness in logarithmic scale ln($S$), and $T$. It should be noted that Zhang *et al.* (2015) had developed a polynomial regression model using those cases with $\delta_{hm}/H_e \leq 1.5\%$ (a total of 1032 of the original

Table 4 Sample data sets of the testing patterns

| $k_{strut}$ (kN/m$^2$) | T (m) | $c_u/\sigma'_v$ | $E_{50}/c_u$ | ln($S$) | $\gamma$(kN/m$^3$) | $\delta_{hm}/H_e$(%) |
|---|---|---|---|---|---|---|
| 31667 | 35 | 0.29 | 100 | 7.313 | 19 | 1.191 |
| 31667 | 30 | 0.34 | 200 | 6.097 | 15 | 1.407 |
| 25333 | 25 | 0.29 | 200 | 7.313 | 17 | 0.827 |
| 42222 | 30 | 0.34 | 300 | 7.313 | 19 | 0.382 |
| 31667 | 35 | 0.34 | 300 | 8.176 | 19 | 0.405 |
| 42222 | 30 | 0.34 | 400 | 8.846 | 19 | 0.241 |
| 25333 | 35 | 0.34 | 100 | 7.313 | 17 | 1.291 |
| 31667 | 30 | 0.34 | 200 | 8.176 | 19 | 0.509 |
| 25333 | 35 | 0.25 | 200 | 7.313 | 17 | 1.273 |
| 31667 | 25 | 0.29 | 200 | 6.097 | 19 | 0.900 |

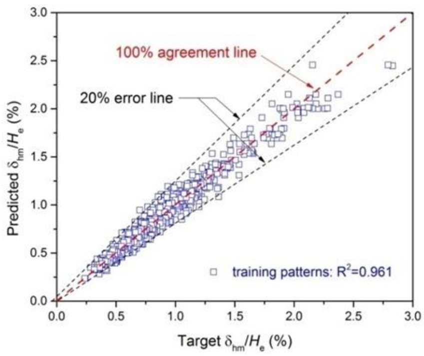


(a)

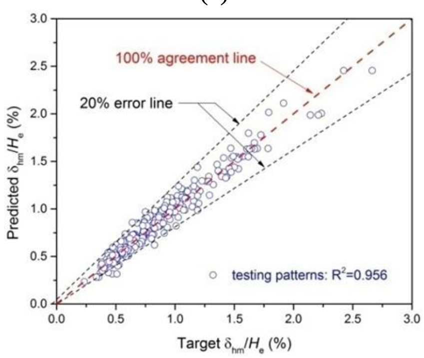


(b)

Fig. 7 Comparison between target and MARS predicted $\delta_{hm}/H_e$, (a) training data and (b) testing data

Table 5 ANOVA decomposition for MARS model

| Function No. | GCV | STD | #basis | variable(s) |
|---|---|---|---|---|
| 1 | 0.011 | 0.052 | 2 | $k_{strut}$ |
| 2 | 0.028 | 0.129 | 2 | $T$ |
| 3 | 0.020 | 0.075 | 2 | $c_u/\sigma'_v$ |
| 4 | 0.049 | 0.181 | 2 | $E_{50}/c_u$ |
| 5 | 0.109 | 0.289 | 2 | ln($S$) |
| 6 | 0.029 | 0.133 | 2 | $\gamma$ |
| 7 | 0.011 | 0.052 | 2 | $T$, $c_u/\sigma'_v$ |
| 8 | 0.008 | 0.028 | 2 | $T$, $E_{50}/c_u$ |
| 9 | 0.010 | 0.043 | 2 | $T$, $\gamma$ |
| 10 | 0.009 | 0.031 | 2 | $c_u/\sigma'_v$,$E_{50}/c_u$ |
| 11 | 0.027 | 0.113 | 3 | $c_u/\sigma'_v$, ln($S$) |

Table 5 Continued

| Function No. | GCV | STD | #basis | variable(s) |
|---|---|---|---|---|
| 12 | 0.009 | 0.030 | 2 | $c_u/\sigma'_v$, $\gamma$ |
| 13 | 0.010 | 0.046 | 3 | $E_{50}/c_u$, ln($S$) |
| 14 | 0.019 | 0.098 | 4 | ln($S$), $\gamma$ |

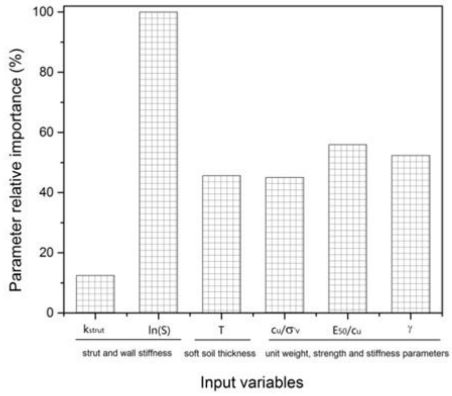


Fig. 8 Relative importance of the input variables in the MARS model

1120 cases) considering that the serviceability limit state is likely to be exceeded for $\delta_{hm}/H_e$ >1.5%. However, a review of measured diaphragm wall displacements from various published case histories of successful deep excavations show that wall deflections can be up to 3% times the excavation depth, without any serviceability problems (Fok *et al.* 2012). Therefore, the results of all 1120 hypothetical cases were used for MARS model building.

Of the 1120 cases, 840 patterns were randomly chosen as the training data sets and the remaining as the testing sets. The criterion of data pattern selection used in this study was based on ensuring that the statistical properties including the mean and standard deviations of the training and testing subsets were similar to each other. Table 4 lists sample data sets of the testing patterns.

The optimal MARS model consisted of 32 BFs of linear spline functions with second-order interaction. A plot of the MARS predicted wall deflection values versus the FEM calculated values for the training and testing patterns is shown in Fig. 7. It can be observed that most of the MARS estimations of the data patterns fell within ±20% of the target values.

Table 5 lists the ANOVA decomposition of the developed model. The first column lists the ANOVA function number. The second column gives an indication of the importance of the corresponding ANOVA function, by listing the GCV score for a model with all BFs corresponding to that particular ANOVA function removed. The third column provides the standard deviation of the function. It gives an indication of its relative importance to the overall model and can be interpreted in a manner similar to the standardized regression coefficient in a linear model. The fourth column gives the number of BFs comprising the ANOVA function. The last column gives the particular input variables associated with the ANOVA function.

Fig. 8 gives the plot of the relative importance of the input variables for the MARS model, which is evaluated by the increase in the GCV value caused by removing the considered variables from the developed MARS model. The results indicate that the normalized maximum wall deflection is more sensitive to the system stiffness ln($S$) compared with the relative soil stiffness ratio $E_{50}/c_u$ and clay unit weight $\gamma$. $k_{strut}$ and ln($S$) represent the structural stiffness of the bracing and supporting systems. $T$, the thickness of clay, can be individually categorized into the excavation geometry since it defines the soil profile. Similarly, unit weight $\gamma$, relative soil stiffness ratio $E_{50}/c_u$ and relative shear strength ratio $c_u/\sigma'_v$ are soil physical and mechanical parameters. For the three categories, the total relative importance values for structural stiffness, excavation geometries and clay physical and mechanical parameters are 112, 46, and 153 %, respectively.

Table 6 lists the BFs and their corresponding equation for the developed MARS model. It is observed from Table 6 that interactions have occurred between BFs (20 of the 32 BFs are interaction terms). These terms include interaction between ln(S) and $\gamma$, ln(S) and $c_u/\sigma'_v$, ln(S) and $E_{50}/c_u$, $T$ and $\gamma$, $T$ and $c_u/\sigma'_v$, $T$ and $E_{50}/c_u$, $\gamma$ and $c_u/\sigma'_v$, $E_{50}/c_u$ and $c_u/\sigma'_v$. The presence of various interactions suggests that the built MARS model is not simply additive and that interactions play a significant role in building an accurate model for normalized maximum wall deflection $\delta_{hm}/H_e$ predictions. This again indicates that MARS is capable of capturing the nonlinear and complex relationships between $\delta_{hm}/H_e$ and a multitude of soil parameters, excavation geometries, and structural stiffness with interactions among each other without making any specific assumption about the underlying functional relationship between the input variables and the dependent response. The equation of MARS normalized maximum wall deflection model is given by

$$
\begin{aligned}
(\delta_{hm}/H_e)^*_{MARS}(\%) &= 0.987 - 0.296\times BF1 + 0.373\times BF2 - 0.0013\times BF3 + 0.0032\times BF4 \\
&-1.68\times BF5 + 4.35\times BF6 - 0.069\times BF7 + 0.113\times BF8 + 0.045\times BF9 - 0.042\times BF10 \\
&-0.054\times BF11 + 0.13\times BF12 + 1.9\times BF13 - 1.7\times BF14 - 9\times 10^{-6}\times BF15 + 7\times 10^{-6}\times BF16 \\
&-0.0007\times BF17 + 0.001\times BF18 - 0.012\times BF19 + 0.011\times BF20 - 0.3\times BF21 + 0.3\times BF22 \\
&+0.037\times BF23 - 0.051\times BF24 + 0.00024\times BF25 - 0.00012\times BF26 + 2.52\times BF27 \\
&+0.265\times BF28 - 0.427\times BF29 + 0.009\times BF30 - 0.005\times BF31 - 0.0008\times BF32
\end{aligned}
\tag{11}
$$

Table 6 Expressions of BFs for MARS model

| BF | Equation | BF | Equation |
|---|---|---|---|
| BF1 | max(0, ln(S)–7.3132) | BF17 | BF2 × max(0, $E_{50}/c_u$–200) |
| BF2 | max(0, 7.3132– ln(S)) | BF18 | BF2 × max(0, 200– $E_{50}/c_u$) |
| BF3 | max(0, $E_{50}/c_u$–200) | BF19 | BF9 × max(0, $\gamma$–17) |
| BF4 | max(0, 200– $E_{50}/c_u$) | BF20 | BF9 × max(0, 17–$\gamma$ ) |
| BF5 | max(0, $c_u/\sigma'_v$–0.25) | BF21 | BF5 × max(0, $T$–30) |
| BF6 | max(0, 0.25–$c_u/\sigma'_v$) | BF22 | BF5 × max(0, 30– $T$) |
| BF7 | max(0, $\gamma$–17) | BF23 | BF1 × max(0, $\gamma$–17) |
| BF8 | max(0, 17–$\gamma$ ) | BF24 | BF1 × max(0, 17–$\gamma$ ) |
| BF9 | max(0, $T$–30) | BF25 | BF4 × max(0, $T$–30) |
| BF10 | max(0, 30– $T$) | BF26 | BF4 × max(0, 30– $T$) |
| BF11 | BF2 × max(0, $\gamma$ –17) | BF27 | BF2 × max(0, 0.29– $c_u/\sigma'_v$) |
| BF12 | BF2 × max(0, 17–$\gamma$ ) | BF28 | BF5 × max(0, $\gamma$–17) |
| BF13 | BF5 × max(0, ln(S)–8.1763) | BF29 | BF5 × max(0, 17–$\gamma$ ) |
| BF14 | BF5 × max(0, 8.1763– ln(S)) | BF30 | BF5 × max(0, $E_{50}/c_u$–300) |

Table 6 Continued

| BF | Equation | BF | Equation |
|---|---|---|---|
| BF15 | max(0, $k_{strut}$ –31667) | BF31 | BF5 × max(0, 300– $E_{50}/c_u$) |
| BF16 | max(0, 31667– $k_{strut}$) | BF32 | BF1 × max(0, 200– $E_{50}/c_u$) |

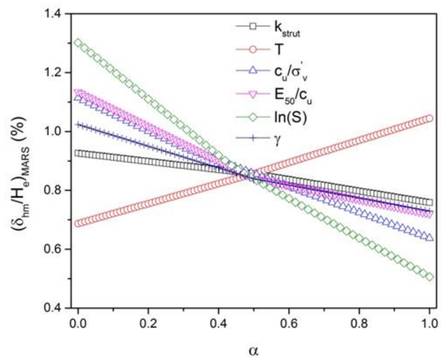


Fig. 9 Effect of all parameters on normalized maximum wall deflection at 0 to 1 scale

In all the previous numerical analyses, the ground water table was assumed at the ground surface, which is considered to be the most unfavourable condition. In many situations with soft clay, the water could be 1-2 m below the ground surface. Additional analyses carried out to investigate the influence of the ground water table indicate that the maximum wall deflection decreases almost linearly with decreasing ground water level. For brevity, these plots have been omitted. The water table correction factor $\mu_w$ can be approximated as $\mu_w = 1 - 0.1l$, where $l$ is the depth of the ground water table below the ground surface (in metres) and $l \leq 2$. Thus, the predicted maximum wall deflection $\delta_{h,PR}$ can be estimated using

$$
(\delta_{hm}/H_e)_{MARS} = \mu_w(\delta_{hm}/H_e)^*_{MARS} \tag{12}
$$

Eqs. (11) and (12) were obtained from multivariate regression analysis of numerical data for excavations in the following ranges: $k_{strut}$ =21111 to 42222kN/m$^2$, $T$ = 25 to 35 m, $c_u/\sigma'_v$=0.21 to 0.34, $E_{50}/c_u$= 100 to 300, ln($S$) = 6.097 to 8.846 and $\gamma$=15 to 19 kN/m$^3$. Therefore, when predicting the normalized maximum wall deflection using the above approaches, it is better that the excavation geometry and soil properties conform to the ranges used in the parametric study.

## 6. Parametric sensitivity analysis

To validate the MARS normalized maximum wall deflection model, a parametric analysis was performed, aiming to find the effect of each input variable on $\delta_{hm}/H_e$. This parametric sensitivity analysis investigates the response of $\delta_{hm}/H_e$ predicted by the MARS model to a set of hypothetical input data generated over the ranges of the minimum and maximum data sets. One input variable was changed each time within its range while the others were kept at the average values of their entire data sets. As suggested by Alavi *et al.* (2011), a set of synthetic data for the single varying parameter was generated by increasing the value of this in increments. These values were presented to the MARS prediction model and $\delta_{hm}/H_e$ was calculated. This procedure was repeated using another variable until the responses of the models were tested for all of the predictor variables (Alavi *et al.* 2011). To better illustrate the effects of all parameters on normalized maximum wall deflection, the range of all parameters is considered in the scale of 0 to 1. An example for changing the range of clay thickness from normal scale to $\alpha$=0 to 1 scale is given in Eq. (13)

$$\alpha_T = \frac{\text{actual clay thickness - lower value (25 m)}}{\text{upper value (35 m) - lower value (25 m)}} \tag{13}$$

The effects of all parameters on $\delta_{hm}/H_e$ on a zero to 1 scale is shown in Fig. 9, plotting the influence of the $\delta_{hm}/H_e$ predictions to the variations of $k_{strut}$, $T$, $c_u/\sigma'_v$, $E_{50}/c_u$, ln($S$) and $\gamma$, respectively. It is obvious that ln(S) influences $\delta_{hm}/H_e$ most, followed by $E_{50}/c_u$ and $\gamma$, while $k_{strut}$ is the least influential factor, which is consistent with the finding in Fig. 8.

## 7. Conclusions

This paper presents a semi-empirical MARS model relating the maximum wall deflection to various parameters including the excavation geometry, soil strength and stiffness parameters, soil unit weight and the wall and strut stiffness. Major findings obtained in this research include:

i) MARS is capable of capturing various interaction terms without making any specific assumption about the underlying functional relationship between the input variables and the response.

ii) MARS is able to provide the relative importance of the input variables and also enables engineers to have better insights and understanding of where significant changes in the data may occur.

It should be noted that since the built MARS model makes predictions based on the knot values and the basic functions, thus interpolations between the knots of design input variables are more accurate and reliable than extrapolations. Consequently, for cases in which the input parameter values are beyond the specific ranges in this study, the proposed MARS model should be used with caution.

## Acknowledgments

A portion of the work was completed while the corresponding author was on sabbatical leave at Nanyang Technological University, Singapore. The corresponding author is grateful to the support by the National Natural Science Foundation of China (No. 51608071), the Advanced Interdisciplinary Special Cultivation program (No.106112017CDJQJ208850).

## References

Addenbrooke, T.I., Potts, D.M. and Dabee, B. (2000), "Displacement flexibility number for multiple retaining wall design", *J. Geotech. Geoenviron. Eng.*, **126**(8), 718-726.

Adoko, A.C., Jiao, Y.Y., Wu, L., Wang, H. and Wang, Z.H. (2013), "Predicting tunnel convergence using multivariate adaptive regression spline and artificial neural network", *Tunn. Undergr. Sp. Tech.*, **38**(3), 368-376.

Alavi, A.H., Ameri, M., Gandomi, A.H. and Mirzahosseini, M.R. (2011), "Formulation of flow number of asphalt mixes using a hybrid computational method", *Constr. Build. Mater.*, **25**(3), 1338-1355.

Alpan, I. (1970), "The geotechnical properties of soils", *Earth Sci. Rev.*, **6**(1), 5-49.

Attoh-Okine, N.O., Cooger, K. and Mensah, S. (2009), "Multivariate adaptive regression spline (MARS) and hinged hyper planes (HHP) for doweled pavement performance modeling", *Constr. Build. Mater.*, **23**(9), 3020-3023.

Benz, T. (2007), "Small-strain stiffness of soil and its numerical consequences", Ph.D. Dissertation, University of Stuttgart, Stuttgart, Germany.

Borja, R.I., Tamagnini, C. and Amorosi, A. (1997), "Coupling plasticity and energy-conserving elasticity models for clays", *J. Geotech. Geoenviron.*, **123**(10), 948-957.

Brinkgreve, R.B.J. and Vermeer, P.A. (1997), *PLAXIS Finite Element Code for Soil and Rock Analysis*, Balkema, Rotterdam, The Neterlands.

Brinkgreve, R.B.J., Broere, W. and Waterman, D. (2006), *PLAXIS Version 8.5 Manual*, Balkema, Rotterdam, The Neterlands.

Bryson, L.S. and Zapata-Medina, D.G. (2012), "Method for estimating system stiffness for excavation support walls", *J. Geotech. Geoenviron.*, **138**(9), 1104-1115.

Burland, J.B. (1989), "Small is beautiful-the stiffness of soils at small strains", *Can. Geotech. J.*, **26**(4), 499-516.

Clayton, C.R.I. (2011), "Stiffness at small strain: Research and practice", *Géotechnique*, **61**(1), 5-37.

Clough, G.W. and O'Rourke, T.D. (1990), *Construction Induced Movements of In Situ Walls*, in *Design and Performance of Earth Retaining Structures*, ASCE, Ithaca, New York, U.S.A., 439-470.

Finno, R.J. and Calvello, M. (2005), "Supported excavations: The observational method and inverse modeling", *J. Geotech. Geoenviron. Eng.*, **131**(7), 826-836.

Finno, R.J. and Tu, X.X. (2006), "Selected topics in numerical simulation of supported excavations", *Proceedings of the International Conference on Numerical Simulation of Construction Processes in Geotechnical Engineering for Urban Environment*, Bochum, Germany, March.

Fok, P., Neo, B.H., Veeresh, C., Wen, D. and Goh, K.H. (2012), "Limiting values of retaining wall displacements and impact to the adjacent structures", *IES J. Part A Civ. Struct. Eng.*, **5**(3), 134-139.

Friedman, J.H. (1991), "Multivariate adaptive regression splines", *Ann. Stat.*, **19**(1), 1-67.

Goh, A.T.C. and Zhang, W.G. (2014), "An improvement to MLR model for predicting liquefaction-induced lateral spread using multivariate adaptive regression splines", *Eng. Geol.*, **170**, 1-10.

Goh, A.T.C., Zhang, Fan., Zhang, W.G., Zhang, Y.M. and Liu, H.L. (2017), "A simple estimation model for 3D braced excavation wall deflection", *Comput. Geotech.*, **83**, 106-113.

Goh, A.T.C., Zhang, W.G., Zhang, Y.M., Xiao, Y. and Xiang, Y.Z. (2016), "Determination of EPB tunnel-related maximum surface settlement: A Multivariate adaptive regression splines approach" *Bull. Eng. Geol. Environ.*, 1-12.

Hashash, Y.M.A. and Whittle, A.J. (1996), "Ground movement prediction for deep excavations in soft clay", *J. Geotech. Geoenviron. Eng.*, **122**(6), 474-486.

Hastie, T., Tibshirani, R. and Friedman, J. (2009), *The Elements of Statistical Learning: Data Mining, Inference and Prediction*, Springer.

Hsieh, P.G. and Ou, C.Y. (2016), "Simplified approach to estimate the maximum wall deflection for deep excavations with cross walls in clay under the undrained condition" *Acta Geotech*., **11**(1),177-189.

Hsieh, P.G., Chien, S.C. and Ou, C.Y. (2012), "A simplified evaluation method for maximum wall deflection induced by deep excavation in clay", *Chin. J. Rock Mech. Eng*., **31**(11), 2285-2290.

Hsieh, Y.M., Dang, P. H., and Lin, H. D. (2016), "How small strain stiffness and yield surface affect undrained excavation predictions", *J. Geomech*., **17**(3), 04016071.

Hsiung, B.C.B., Yang, K.H., Aila, W. and Hung, C. (2016), "Three dimensional effects of a deep excavation on wall deflections in loose to medium dense sands", *Comput. Geotech*., **80**, 138-151.

Jardine, R.J., Potts, D.M., Fourie, A.B. and Burland, J.B. (1986), "Studies of the influence of non-linear stress-strain characteristics in soil-structure interaction", *Géotechnique*, **36**(3), 377-396.

Jekabsons, G. (2010), *VariReg: A Software Tool for Regression Modeling Using Various Modeling Methods*, Riga Technical University, <http://www.cs.rtu.lv/jekabsons/>.

Jen, L.C. (1998), "The design and performance of deep excavation in clay", Ph.D. Dissertation, Massachusetts Institute of Technology, Cambridge, Massachusetts, U.S.A.

Khoshnevisan, S., Juang, H., Zhou, Y.G. and Gong, W. (2015), "Probabilistic assessment of liquefaction-induced lateral spreads using CPT-Focusing on the 2010-2011 Canterbury earthquake sequence", *Eng. Geol*., **192**, 113-128

Koutsoftas, D.C. (2012), "State of practice: Excavations in soft soils", *Proceedings of the Geocongress 2012: State of the Art and Practice in Geotechnical Engineering*, Oakland, California, March.

Kung, G.T.C. (2003), "Surface settlement induced by excavation with consideration of small-strain behavior of Taipei silty clay", Ph.D. Dissertation, National University of Science and Technology, Taipei, Taiwan.

Kung, G.T.C., Hsiao, E.C.L. and Juang, C.H. (2007b), "Evaluation of a simplified small-strain soil model for analysis of excavation-induced movements", *Can. Geotech. J*., **44**(6), 726-736.

Kung, G.T.C., Juang, C.H., Hsiao, E.C.L. and Hashash, Y.M.A. (2007a), "Simplified model for wall deflection and ground-surface settlement caused by braced excavation in clays", *J. Geotech. Geoenviron. Eng*., **133**(6), 731-747.

Kung, G.T.C., Ou, C.Y. and Juang, C.H. (2009), "Modeling small-strain behavior of Taipei clays for finite element analysis of braced excavations", *Comput. Geotech*., **36**(1), 304-319.

Lam, S.S.Y. (2010), "Ground movements due to excavation in clay: Physical and analytical models", Ph.D. Dissertation, University of Cambridge, Cambridge, U.K.

Lashkari, A. (2012), "Prediction of the shaft resistance of non-displacement piles in sand", *J. Numer. Anal. Met*., **37**(8), 904-931.

Lashkari, A. and Mahboubi, M. (2015), "Use of hyper-elasticity in anisotropic clay plasticity models", *Sci. Iran*., **22**(5), 1643-1660.

Long, M. (2001), "Database for retaining wall and ground movements due to deep excavations", *J. Geotech. Geoenviron. Eng*., **127**(3), 203-224.

Mana, A.I. and Clough, G.W. (1981), "Prediction of movement for braced cuts in clay", *J. Geotech. Geoenviron. Eng.*, **107**(6), 759-777.

Moormann, C. (2004), "Analysis of wall and ground movements due to deep excavations in soft soil based on a new worldwide database", *Soil. Found*., **44**(1), 87-98.

Osman, A.S. and Bolton, M.D. (2006), "Ground movement predictions for braced excavations in undrained clay", *J. Geotech. Geoenviron. Eng*., **132**(4), 465-477.

Poh, T.Y., Wong, I.H. and Chandrasekaran, B. (1997), "Performance of two propped diaphragm walls in stiff residual soils", *J. Perform. Construct. Fac*., **11**(4), 190-199.

Rampello, S., Viggiani, G.M.B. and Amorosi, A. (1997), "Small-strain stiffness of reconstituted clay compressed along constant triaxial effective stress ratio paths", *Géotechnique*, **47**(3), 475-489.

Samui, P. and Karup, P. (2011), "Multivariate adaptive regression spline and least square support vector machine for prediction of undrained shear strength of clay", *J. Appl. Math. Comput*., **3**(2), 33-42.

Schanz, T., Vermeer, P.A. and Bonnier, P.G. (1999), *The Hardening Soil Model-Formulation and Verification*, in *Beyond 2000 in Computational Geotechnics*, Balkema, Amsterdam, The Netherlands.

Son, M. and Cording, E.J. (2005), "Estimation of building damage due to excavation-induced ground movements", *J. Geotech. Geoenviron. Eng*., **131**(2), 162-177.

Ukritchon, B., Whittle, A.J. and Sloan, S.W. (2003), "Undrained stability of braced excavations in clay", *J. Geotech. Geoenviron. Eng*., **129**(8), 738-755.

Vucetic, M. and Dobry, R. (1991), "Effect of soil plasticity on cyclic response", *J. Geotech*., *Eng*., **117**(1), 89-107.

Wang, J.H., Xu, Z.H. and Wang, W.D. (2010), "Wall and ground movement due to deep excavations in Shanghai soft soils", *J. Geotech. Geoenviron. Eng*., **136**(7), 985-994.

Whittle, A.J. Corral, G., Jen, L.C. and Rawnsley, R.P. (2014), "Prediction and performance of deep excavations for courthouse station, Boston", *J. Geotech. Geoenviron. Eng*., **141**(4), 04014123.

Wong, K.S. and Broms, B.B. (1989), "Lateral wall deflections of braced excavation in clay", *J. Geotech. Eng*., **115**(6), 853-870.

Wroth, C.P. and Houlsby, G.T. (1985), "Soil mechanics-property characterization and analysis procedures", *Proceedings of the 11th International Conference on Soil Mechanics and Foundations Engineering*, San Francisco, California, U.S.A., August.

Xuan, F. (2009), "Behaviour of diaphragm walls in clays and reliability analysis", M.Sc. Dissertation, Nanyang Technological University, Nanyang, Singapore.

Yoo, C.S. and Kim, Y.J. (1999), "Measured behaviour of in situ walls in Korea", *Proceedings of the 5th International Symposium on Field Measurements in Geomechancis*, Balkema, Amsterdam, The Netherlands.

Zarnani, S., El-Emam, M. and Bathurst, R.J. (2011), "Comparison of numerical and analytical solutions for reinforced soil wall shaking table tests", *Geomech. Eng*., **3**(4), 291-321.

Zhang, W.G. and Goh, A.T.C. (2013), "Multivariate adaptive regression splines for analysis of geotechnical engineering systems", *Comput. Geotech*., **48**, 82-95.

Zhang, W.G. and Goh, A.T.C. (2016), "General behavior of braced excavation in Bukit Timah Granite residual soils: A case study", *J. Geoeng. Case Histor*., **3**(3), 190-202.

Zhang, W.G., Goh, A.T.C. and Xuan, F. (2015), "A simple prediction model for wall deflection caused by braced excavation in clays", *Comput. Geotech*., **63**, 67-72.

Zhang, W.G., Goh, A.T.C., Zhang, Y.M., Chen, Y.M. and Xiao, Y. (2015), "Assessment of soil liquefaction based on capacity energy concept and multivariate adaptive regression splines", *Eng. Geol*., **188**, 29-37.

Zhang, W.G., Zhang, Y.M. and Goh, A.T.C. (2017), "Multivariate adaptive regression splines for inverse analysis of soil and wall properties in braced excavation", *Tunn. Undergr. Sp. Tech*., **64**, 24-33.

*CC*